Transient binding of dynein controls bidirectional long-range motility of early endosomes

Martin Schuster[a], Reinhard Lipowsky[b], Marcus-Alexander Assmann[c], Peter Lenz[c], and Gero Steinberg[a,1]

[a]Department of Biosciences, University of Exeter, Exeter EX4 4PE, United Kingdom; [b]Department of Theory and Bio-Systems, Max Planck Institute of Colloids and Interfaces, D-14424 Potsdam, Germany; and [c]Fachbereich Physik and Zentrum für Synthetische Mikrobiologie, Philipps University Marburg, D-35032 Marburg, Germany

Edited by J. Richard McIntosh, University of Colorado, Boulder, CO, and approved January 7, 2011 (received for review November 3, 2010)

In many cell types, bidirectional long-range endosome transport is mediated by the opposing motor proteins dynein and kinesin-3. Here we use a fungal model system to investigate how both motors cooperate in early endosome (EE) motility. It was previously reported that Kin3, a member of the kinesin-3 family, and cytoplasmic dynein mediate bidirectional motility of EEs in the fungus *Ustilago maydis*. We fused the green fluorescent protein to the endogenous dynein heavy chain and the *kin3* gene and visualized both motors and their cargo in the living cells. Whereas kinesin-3 was found on anterograde and retrograde EEs, dynein motors localize only to retrograde organelles. Live cell imaging shows that binding of retrograde moving dynein to anterograde moving endosomes changes the transport direction of the organelles. When dynein is leaving the EEs, the organelles switch back to anterograde kinesin-3–based motility. Quantitative photobleaching and comparison with nuclear pores as an internal calibration standard show that single dynein motors and four to five kinesin-3 motors bind to the organelles. These data suggest that dynein controls kinesin-3 activity on the EEs and thereby determines the long-range motility behavior of the organelles.

membrane trafficking | modeling

Intracellular transport of organelles, proteins, or mRNA is common in eukaryotes (1, 2). It is usually bidirectional, which is thought to help motors to bring their cargo to the right destination (3). Intracellular transport is mediated by motor proteins belonging to the kinesins and dyneins that bind to the organelles and hydrolyze ATP to move their cargo along the microtubules (MTs) (4). Most kinesins "walk" toward the plus ends of the MTs, whereas dynein takes its cargo to the minus ends. Their collective activities organize and distribute organelles within the cell or transmit information. Motor-based cargo transport is of particular importance for highly polarized cells such as filamentous fungi and neurons and, consequently, many neuronal disorders are related to defects in axonal transport (5).

Bidirectional motility is thought to be governed by teams of opposing dynein and kinesin motors, which are tightly bound to the organelle or vesicle (1, 2). Quantitative analyses of motor numbers in living cells have shown that a few motors of each type bind to the same organelle, where they coordinate and control each other's activity (3, 6, 7). The number of bound motors is remarkably similar in different systems, usually ranging from one to five motors of each type (7–10), although in a few cases larger numbers were also reported (11, 12). The presence of both kinesin and dynein on a cargo implies that both motors may be pulling on the cargo at the same time, which leads to essentially no motion of the cargo. Bidirectional transport, in which the cargo switches from plus motion to minus motion and vice versa, could be induced by a putative coordination complex that ensures that only one of the two motor teams is active at a given time (1). However, such a coordination complex has not yet been identified. Instead, bidirectional motility can arise from a stochastic tug-of-war, in which the number of actively pulling motors changes by fluctuations (13). Regulatory proteins could influence such stochastic tug-of-war and can lead to a large variety of transport patterns. Indeed, strong evidence from work on *Drosophila* lipid droplets (8, 9, 14) or peroxisomes (11) and melanosome movement (6) demonstrates that kinases (15, 16), dynactin (17), and other factors (8, 18, 19) control bidirectional membrane trafficking.

In this study we use the genetically tractable fungal model system *Ustilago maydis* to analyze the role of motors and MTs in long-range transport of early endosomes (EEs). This fungus provides a broad spectrum of technical advantages and shares remarkable similarity with human cells (20). Among the genes that are conserved between humans and *U. maydis* are several components of the MT-based transport machinery in neurons, such as kinesin-1, kinesin-3, and the dynein light chain roadblock. In mammalians these proteins are required for long-distance transport of membranes (4, 21) and similar roles were suggested in *U. maydis* (22). In this fungus, the only membranous cargo known to travel in a bidirectional fashion along MTs is EEs (23). Similar to that in humans (24) and amoebas (10), kinesin-3 motors carry the EEs to MT plus ends at the hyphal tip (anterograde motility) (25, 26), where they support polarized growth and mating by local endocytic recycling (23, 27). The importance of the retrograde dynein-driven EE motility is unknown, but it might mediate communication with the nucleus (28).

In previous studies of bidirectional transport, it was assumed, either implicitly or explicitly, that motors of opposing activity simultaneously attach to the cargo. By visualizing native levels of dynein and kinesin-3 during their interaction with the EEs we have discovered an unexpected mechanism by which these motors cooperate. We provide unique experimental evidence that organelle motility can be controlled by loading motors during a cargo run.

Results

Early Endosomes Switch Between Long Phases of Anterograde and Retrograde Motility. In the elongated hyphal cells of the fungus (Fig. 1*A*) EEs move bidirectionally along MTs (26). Dynein is concentrated at MT plus ends in the growing cell tip (26) (Fig. 1*A*, growth region indicated by asterisk), and it was suggested that dynein stays there to receive arriving EEs for retrograde transport back toward the cell center. If the apical dynein accumulation serves as a loading zone, all EEs have to reach the hyphal tip before changing direction. We tested this by visualizing anterograde motility of photoactivatable green fluorescent protein (paGFP) fused to the small endosomal GTPase Rab5a, which has been shown to localize to EEs in *U. maydis* (27). The use of this GFP variant enabled us to visualize subsets of EEs and reduced interferences. When activated by a pulse of 405 nm laser light near the nucleus (Fig. 1*A*, arrowhead, 405 nm), the EEs became visible, moving over long distances toward the MT plus ends in the hyphal tip before they changed direction for

Author contributions: M.S. and G.S. designed research; M.S., M.-A.A., and P.L. performed research; M.S., R.L., and G.S. analyzed data; and G.S. wrote the paper.

The authors declare no conflict of interest.

This article is a PNAS Direct Submission.

[1]To whom correspondence should be addressed. E-mail: g.steinberg@exeter.ac.uk.

This article contains supporting information online at www.pnas.org/lookup/suppl/doi:10.1073/pnas.1015839108/-/DCSupplemental.

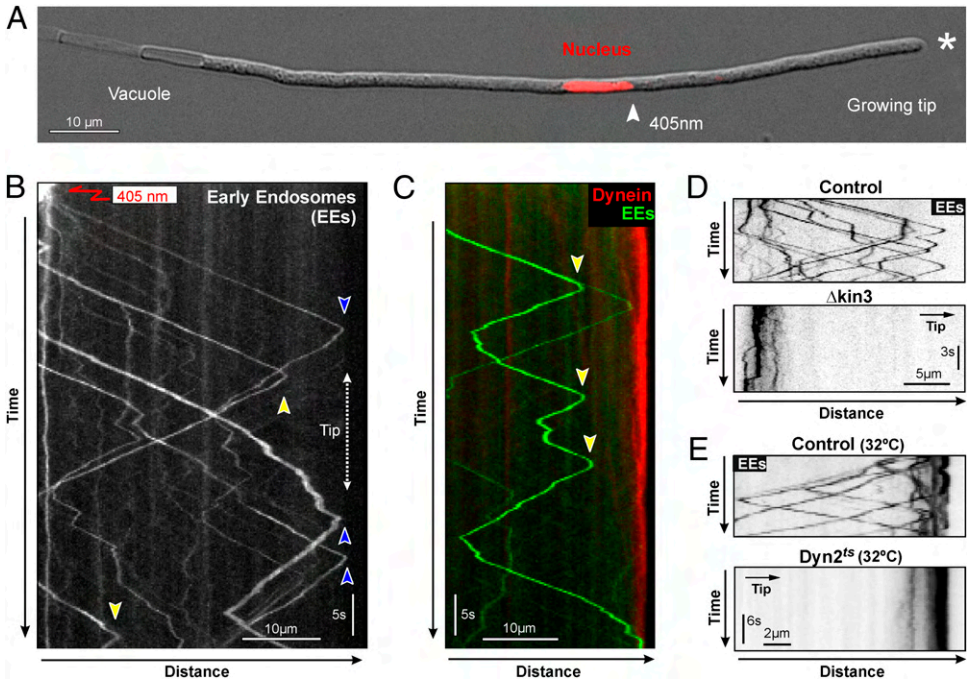

Fig. 1. Motility of early endosomes in *U. maydis*. (*A*) Hyphal cell of *U. maydis*. The centrally positioned nucleus was labeled with monomeric red fluorescent protein fused to a nuclear localization signal. The arrowhead indicates the point of photoactivation of paGFP-Rab5a by a 405-nm laser. (*B*) Kymograph showing motility of activated paGFP-Rab5a bound to EEs. The red arrow indicates the point of activation by a local 405-nm laser pulse. Anterograde-to-retrograde turning points are indicated by blue and yellow arrowheads. See also Movie S1. (*C*) Kymograph showing bidirectional motility of few paGFP-Rab5a bound to EEs and endogenous dynein, labeled by mCherry fused to the endogenous dynein heavy chain gene. (*D*) Kymograph of anterograde motility of paGFP-Rab5a in control cells (Control) and kinesin-3 null cells (Δkin3). Contrast was inverted. (*E*) Kymographs showing retrograde motility of paGFP-Rab5a in control cells (Control) and in temperature-sensitive dynein mutants (Dyn2^{ts}) at restrictive temperature (32 °C). Contrast was inverted.

retrograde motility (Fig. 1*B*, blue arrowheads, and Movie S1). Despite a minor difference in velocity, no significant disparity was found in run length, flux, or pausing between anterograde and retrograde EEs (Table S1). The majority of the EEs (~74%, n = 321) changed from anterograde to retrograde before reaching the hyphal tip (Fig. 1*B*, yellow arrowheads), suggesting that they have not reached the dynein comets at the apical MT plus ends. Indeed, coexpression of paGFP-Rab5a and a fusion protein of a triple-mCherry3 tag and the endogenous dynein heavy chain gene demonstrated that EEs frequently reversed direction without meeting the apical dynein accumulation (Fig. 1*C*, anterograde to retrograde turning indicated by arrowheads). This oscillatory motility of EEs was reminiscent of a stochastic switching of transport direction as proposed by the tug-of-war scenario (13).

Kinesin-3 and Dynein Mediate Bidirectional Endosome Transport. It was previously shown that the steady-state distribution of EEs depends on kinesin-3 and dynein, suggesting that both motors participate in bidirectional EE trafficking (25, 26). Indeed, when paGFP-Rab5a was photoactivated in subapical regions of kinesin-3 null mutant hyphae, no anterograde motility of EEs was observed (Fig. 1*D*, Δkin3). Similar photoactivation in hyphae expressing a conditional allele of dynein heavy chain revealed a block in retrograde vesicle motility (Fig. 1*E*, Dyn2^{ts}). We therefore conclude that kinesin-3 and dynein mediate long-range EE motility. To better understand how kinesin-3 and dynein mediate bidirectional EE trafficking we set out to visualize the motors underlying this motility. We fused a triple GFP tag to the endogenous dynein heavy chain gene *dyn2*, which is essential for cell survival in *U. maydis* (29). The use of a triple-tandem repeat of GFP enabled us to visualize the otherwise faint signals traveling along the MTs. Fusing tags to Dyn2 did not cause any growth defect (Fig. S1, GFP$_3$-Dyn2; compare with the conditional dynein mutant, Dyn2^{ts}), indicating that the GFP-fusion proteins were functional. We found numerous fluorescent signals that moved bidirectionally in all parts of the hyphal cell (Fig. 2*A*, retrograde, red arrowheads; anterograde, blue arrowheads; and Movie S2). Previous work has shown that the apical concentration of dynein at MT plus ends depends on fungal kinesin-1 (26, 30), suggesting that the anterograde motility of dynein reflects kinesin-1 delivery to MT plus ends near the cell tip, whereas dynein moves in a retrograde direction on its own. To better visualize retrograde dynein motility, we photobleached a region behind the hyphal tip and observed dynein signals processively moving from the tip into this bleached subapical area (Fig. 2*B*). This treatment did not affect the motility of the motors. We next set out to visualize kinesin-3. We did not succeed in fusing a triple-GFP tag to kinesin-3, but managed to generate a fusion of *kin3*, which encodes kinesin-3 in *U. maydis* (25) and single GFP. When expressed under the native *kin3* promoter, these native levels of kinesin-3–GFP were able to rescue the deletion phenotype, suggesting that the fusion protein is biologically active (Fig. S1, Δ*kin3*). In hyphae kinesin-3–GFP showed rapid long-range motility, which again was best visible when parts of the cell were pretreated with 405 nm laser light to clear the region of interfering signals (Fig. 2*C* and Movie S3). We frequently observed kinesin-3–GFP signals that reversed direction (Fig. 2*D* and Movie S4). To test whether the motor is attached to anterograde and retrograde EEs we coexpressed kinesin-3–GFP and a red-fluorescent mCherry-Rab5a fusion protein. Indeed, kinesin-3 was found on anterograde (Movie S5) and on retrograde EEs (Fig. 2*E*). Less than 2% of all kinesin-3 signals did not colocalize with EEs (n = 326 anterograde signals and 482 retrograde signals). In contrast, dynein was absent from most anterograde moving EEs (97% without dynein, n = 102; Fig. 2*F* and Fig. S2), whereas retrograde moving EEs colocalized with dynein (93.5%, n = 107; Fig. 2*G* and Movie S6). In addition, some dynein signals moved toward MT minus ends without carrying EEs (Fig. 2*G*, arrowhead). Therefore, we conclude that kinesin-3 is always bound to the cargo, whereas dynein is associated only with retrograde EEs and is not a passive cargo on anterograde moving EEs.

Single Dynein Opposes Several Kinesin-3 Motors. We next set out to obtain quantitative information about the number of motors involved in motility of single EEs. Protein numbers can be determined by an analysis of their bleaching behavior (7, 31–33). To apply this method to our living cells we had to immobilize the rapidly moving GFP$_3$–dynein and kinesin-3–GFP signals so that the signals stay in focus while being observed with a 488-nm laser. We did this by mild treatment with carbonyl cyanide 3-chlorophenyl-hydrazone (CCCP), a drug that reversibly inhibits cell respiration resulting in reduced ATP levels (34). This treatment stopped dynein and kinesin-3 motility and anchored the

CELL BIOLOGY

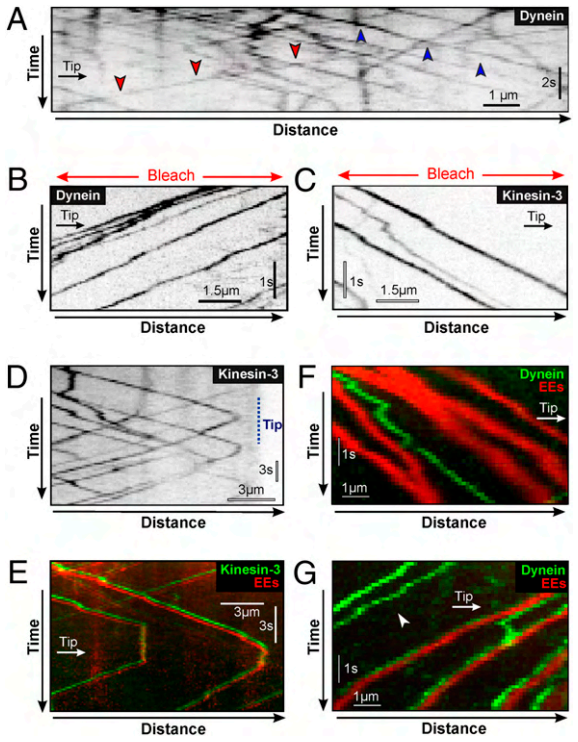

Fig. 2. Motility of molecular motors and their cargo. (*A*) Kymograph showing bidirectional motility of GFP_3–dynein heavy chain. Retrograde motility is indicated by red arrowheads; anterograde motility is indicated by blue arrowheads. Position of cell tip is indicated by "Tip". See also Movie S2. (*B*) Kymograph showing retrograde motility of GFP_3–dynein heavy chain at a high frame rate. Note that the movement is processive. Prebleached area is indicated by a red arrow. Contrast was inverted. See also Movie S2. (*C*) Kymograph showing anterograde motility of kinesin-3–GFP at a high frame rate. Prebleached area is indicated by a red arrow. Contrast was inverted. (*D*) Kymograph of kinesin3-GFP turning direction near the cell tip. Contrast was inverted. See also Movie S3. (*E*) Kymograph of kinesin3-GFP (green) and mCherry-Rab5a (red) colocalizing on bidirectionally moving EEs. Images were slightly offset in the *y* direction to better demonstrate colocalization. See also Movie S5. (*F*) Kymograph of GFP_3–dynein heavy chain and mCherry-Rab5a on anterograde EEs. Dynein is not present on EEs that move toward the tip. (*G*) Kymograph of GFP_3–dynein heavy chain and mCherry-Rab5a on retrograde EEs. Some retrograde moving dynein is not bound to EEs (arrowhead). See also Movie S6.

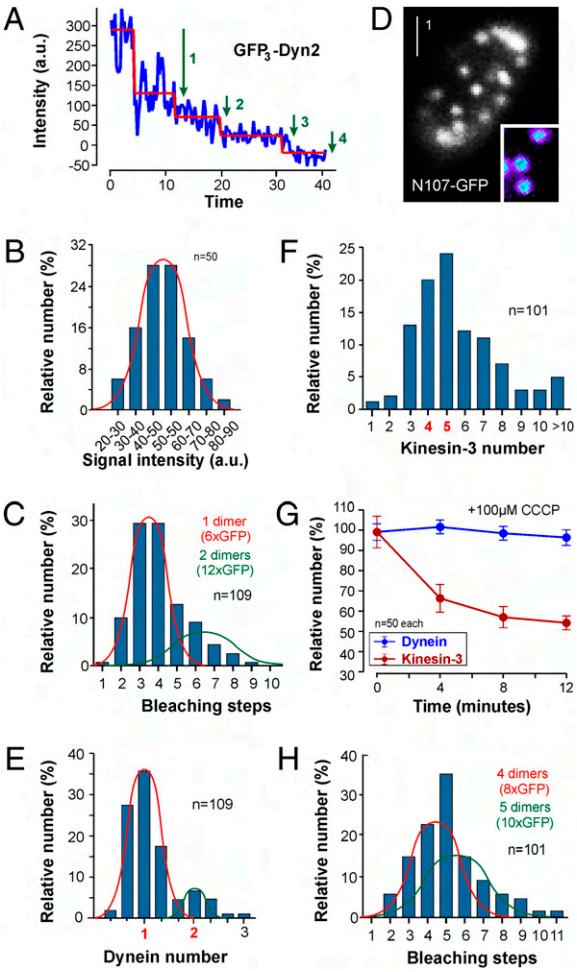

Fig. 3. Determination of motor numbers. (*A*) Bleaching curve and bleaching steps estimated for GFP_3-Dyn2 by the algorithm STEPFINDER. (*B*) Bar chart showing the distribution of bleaching steps for GFP_3-Dyn2, estimated by the algorithm STEPFINDER. (*C*) Bar chart showing bleaching steps of GFP_3–dynein heavy chains on retrograde EEs. Most signals bleached in 1–6 steps (red curve), indicating single dimers of the heavy chain that was fused to a triple-GFP tag. (*D*) Nuclear pores labeled with a fusion protein of the endogenous nuclear porin Nup107 and GFP. Pores contain 16 copies of the fusion protein and individual pores show an even fluorescence (*Inset*, intensity given in pseudocolors). (*E*) Bar chart showing dynein numbers on retrograde EEs, estimated from comparison of GFP_3–dynein heavy chain signals with Nup107-GFP. Again, the majority of the signals represent a single dynein motor. (*F*) Bar chart showing kinesin-3 numbers on anterograde EEs, estimated from comparison of kinesin-3–GFP signals in the first frame of video sequences with Nup107-GFP. Three to six dimeric motors are estimated to bind to the organelle. (*G*) Graph showing GFP3–dynein and kinesin-3–GFP intensities in the presence of 100 μM CCCP. Note that comparison with Nup107-GFP indicates that the kinesin-3–GFP signal at $T = 0$ min corresponds to five dimers. Bleaching was taken into account. (*H*) Bar chart showing bleaching steps of kinesin-3–GFP on anterograde EEs. Most signals bleach in 1–11 steps, which represents two normal distributions (red and green curve), suggesting that most EEs carry four or five dimeric motors.

motors to the MTs, but did not kill the cells because motility could be restored by removing the drug with fresh medium (Fig. S3 *A* and *B*). To distinguish between anterograde and retrograde dynein signals, we applied the drug after they traveled into photobleached regions (*SI Methods*). Indeed, we found that signals bleached in distinct steps (identified by the algorithm STEPFINDER) (35) (Fig. 3*A*). The size of the steps varied, indicating that individual steps are due to bleaching of either single or multiple GFPs. The reduction in fluorescence intensity for the smallest steps followed a Gaussian distribution (Fig. 3*B*), suggesting that they represent bleaching of one GFP. Consequently, large step sizes are likely to be due to bleaching of several GFP molecules (e.g., three GFPs for step 1 in Fig. 3*A*). Bleaching of GFP_3–dynein occurred in one to six steps (Fig. 3*C*), indicating that the signals come from 6× GFP, which represents two triple-GFP tags fused to the dynein heavy chain.

We confirmed these results by using a fusion protein of GFP to the endogenous nuclear porin Nup107 and used this as an internal calibration standard. Nuclear pores became visible (Fig. 3*D*) that contained 16 of the Nup107-GFP proteins (36). Individual pores show an even fluorescence intensity (Fig. 3*D*, *Inset*; fluorescence intensity given in pseudocolors) and the average fluorescence intensity of a single Nup107-GFP corresponded to the reduction in fluorescence intensity in a single photobleaching step (loss per bleaching step, 50.45 ± 1.91 arbitrary units, $n = 50$; intensity of one GFP in nuclear pore calibration, 50.63 ± 1.25 arbitrary units, $n = 50$; not different, $P = 0.9366$). Using GFP-Nup107 as a standard, we estimated the intensity of the majority of GFP_3–dynein signals coming from six GFP tags (Fig. 3*E*). These data confirm that single dynein motors move along MTs. In contrast to dynein, kinesin-3–GFP signals were much stronger

and varied in intensity. We measured the fluorescence intensity of anterograde kinesin-3–GFP in video sequences by comparing anterograde signals to Nup107-GFP. Assuming that kinesin-3 dimerizes (33), this analysis indicates four to six kinesin-3 motors bound to a single EE (Fig. 3*F*). We set out to confirm this result by a bleaching step analysis of CCCP-immobilized signals. However, the stationary kinesin-3–GFP signals lost intensity with time in CCCP (Fig. 3*G*) and according to the internal calibration standard were dropping from five to three kinesin-3–GFPs. In contrast, GFP_3–dynein signal intensities remained stable over time (Fig. 3*G*). Therefore, we consider it possible that only a subset of kinesin-3 motors is anchored to MTs in the presence of CCCP. To obtain more stable signals for bleaching step analysis, we mildly fixed the cells with 0.1% formaldehyde, which immobilized the signals within a few minutes. Under these conditions kinesin-3–GFP photobleached in 2–11 steps, corresponding to four to five kinesin-3 dimers (Fig. 3*H*). Taken together, these data demonstrate that we were able to visualize single motors in the living cell, which revealed that one dynein supports retrograde EE transport, whereas anterograde movement might involve three to five kinesin-3 dimers.

In Vivo Observation of Cargo and Motors Supports an "On-the-Run" Loading of EEs. Dynein concentrates at MT plus ends, which are enriched at the cell tip, but are also found in subapical parts of the cell (26). It was suggested that this dynein accumulation serves as a reservoir of motors that capture arriving EEs for retrograde motility (26). In this study we show that the majority of the anterograde EEs change transport direction before reaching the dynein at the hyphal tip. There are two possible explanations for this behavior: (*i*) EEs change transport direction at subapical dynein accumulations formed at cytoplasmic MT ends or (*ii*) dynein takes over while EEs are traveling toward MT plus ends (on-the-run loading). We tested this result by observing paGFP-Rab5a carrying EEs in cells expressing mCherry-dynein. In kymographs a significant portion of the EEs changed transport direction independent of any dynein accumulation (Fig. 4*A*, event "2"; subapical dynein accumulation at tips of growing MTs indicated by blue arrowheads), which occurred over the whole length of the hypha (Fig. 4*B*), suggesting that EEs indeed interact with dynein while moving toward MT plus ends.

If the change in transport direction of EEs near the nucleus is a consequence of an on-the-run loading of EEs, dynein motors that leave the apical MT plus ends need to travel over long distances to meet the anterograde EEs. To measure the retrograde run length of dynein we made use of a strain in which the endogenous copy of the dynein heavy chain is fused to 3× photoactivatable GFP (paG_3Dyn2) (36). After activation at the hyphal tip using a 405-nm laser pulse, paG_3Dyn2 signals became visible. These signals traveled toward the cell center (Fig. 4*C*, red arrowheads) and usually disappeared after ∼10 μm (median: 12.36 μm; Fig. S4). However, ∼24% of all dynein signals moved over distances >20 μm and maximum run length was found to be 44.5 μm. These experiments suggest that dynein has the capacity to move over long distances, which could support a change in EE transport direction in subapical regions of the cell.

The data presented suggest that EEs meet dynein, which gets loaded while the organelles are on the run. If this assumption is true, we expected to see such a loading mechanism when visualizing GFP-labeled dynein and mCherry-Rab5a–labeled EEs. We did these experiments in regions that were prebleached by 405 nm laser light to clear the cell from interfering signals. We observed anterograde moving EEs meeting retrograde moving dynein signals on single tracks. In most cases (242 of 247 events in 30 cells) dynein passed by the EEs. However, 2.02% of all dynein (5 of 247 events) continuously colocalized with the EEs, which in all cases led to a turn from anterograde to retrograde motility [Fig. 5 *A* and *B* (Loading) and Movie S7]. These findings suggest that dynein bound to the EEs and forced a change in transport direction. We did numerous additional experiments (>200 cells) and collected further collision events. Analyzing

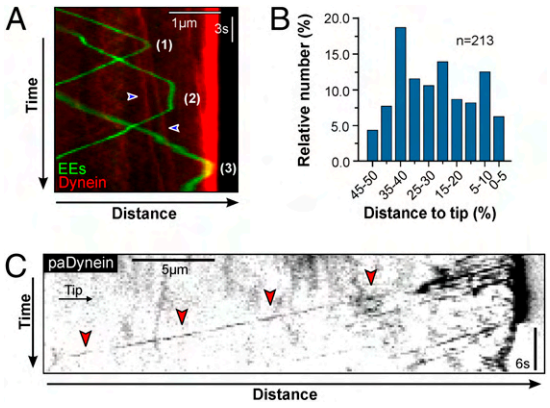

Fig. 4. Anterograde-to-retrograde turning of photoactivated EEs and run length of photoactivated dynein. (*A*) Kymographs showing $mCherry_3$-dynein (red) at the hyphal tip (3) and at subapical plus ends (blue arrowheads) that appear as diagonal lines due to the slow elongation of the MTs. EEs (green) turn at the apical dynein accumulation (3), at subapical dynein comets (1), but also without reaching any dynein concentration (2). (*B*) Bar chart showing anterograde-to-retrograde turning of paGFP-Rab5a EEs, activated near the nucleus. (*C*) Kymograph showing retrograde motility of paG_3Dyn2 after activation with a 405-nm laser. Occasionally dynein signals traveled in a retrograde direction for >25 μm (red arrowheads). Contrast was inverted.

these revealed that turning happened after 111.4 ± 127.8 ms (n = 35 binding events; Fig. 5*C*). Release of dynein from the EEs either resulted in a retrograde-to-anterograde turn (61.5%, n = 52) [Fig. 5 *A* (*Upper*, Release) and *B* (Release, Antero) and Movie S7] or led to a pause for >0.75 s [Fig. 5 *A* (*Lower*, Release), *B* (Release, Pause), and *C*] that often was accompanied by Brownian motion. This behavior indicates that EEs have lost contact with their track. Occasionally, pausing was followed by continued retrograde motility without dynein binding, suggesting that kinesin-3 is able to move retrogradely in subapical regions where MTs are antipolar (26). Finally, we noted that the kinesin-3 signal varied in intensity during anterograde and retrograde movement (Movie S8). We quantified this effect in anterograde kinesin-3 spots and in most cases (73.3%, n = 30) found a transient decrease in signal intensity before a change in transport direction (Fig. 5*D*). Changes in motor numbers are predicted to have a significant influence on the balance of forces during tug-of-war (13). The transient reduction of kinesin-3 motor might therefore foster dynein to bind to membranes and/or to win over kinesin-3 in a tug-of-war.

Discussion

Many cellular cargos display bidirectional motion along microtubules (1, 2). This motility is powered by the opposing motor complexes kinesin and dynein (4). These motors simultaneously bind to their cargo, which was shown in various cell systems, including fish and frog melanosomes (37), amoebas (38), lipid droplets in flies (14), intraflagellar transport in worms and algae (39, 40), and vesicles in mammalian axons (41, 42). The concurrent presence of kinesin and dynein is thought to be crucial for motor activity (3, 13, 43), but also recycles the motor back to MT plus ends (39, 41). In fungi, kinesin-1 is thought to be involved in this process (26, 30), making it likely that the observed anterograde motility of dynein is due to kinesin-1 activity. It remains to be seen whether both motors directly interact (42) or attach to the same membranous cargo (41).

Bidirectional motility can be explained by a tug-of-war scenario (44), where the cargo can be pulled by two different motor teams that simultaneously bind to the membrane. This concept gained recent experimental support (7, 10), and our observations on the long-range EE motility in *U. maydis* are consistent with an extended tug-of-war scenario, in which the EE is pulled by kinesin-3 and dynein, but the presence of dynein varies with time.

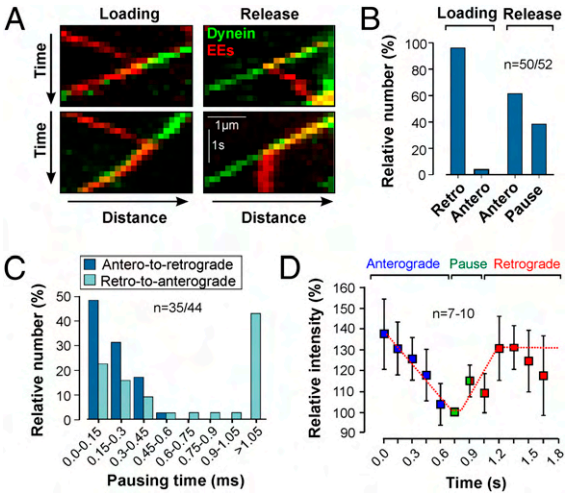

Fig. 5. Role of kinesin-3 and dynein in reversing the direction of endosome motility. (*A*) Kymographs showing the dynamic interaction of dynein (green) and EEs (red). Binding of dynein results in anterograde-to-retrograde turning (Loading), whereas dynein release results in either retrograde-to-anterograde turning or pausing (Release). See also Movie S7. (*B*) Bar chart of relative number of turnings when dynein binds to (Loading) or unbinds from (Release) the EEs. Binding of dynein triggers retrograde motion (Loading, Retro), whereas unbinding is followed by anterograde motility (Release, Antero) or a pause (Release, Pause). Note that pausing of EEs was occasionally followed by retrograde motility in the absence of dynein. (*C*) Histogram showing pausing times at anterograde-to-retrograde turnings and retrograde-to-anterograde turnings. Note that all immobile EEs carried kinesin-3 (n = 26). (*D*) Graph showing relative kinesin-3–GFP intensity prior to (Anterograde, blue) and after (Retrograde, red) turning. Signals that are immobile or randomly diffuse are considered to be in pause (Pause, green). Values are mean ± SEM (n = 7–10 per data point).

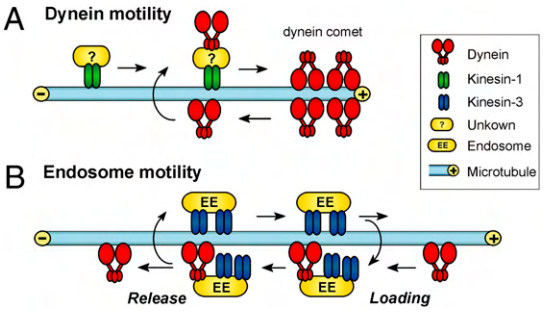

Fig. 6. Model for the interaction of kinesin-3 and dynein during bidirectional EE motility. (*A*) Kinesin-1 delivers dynein to the MT plus end, where dynein forms a comet (26). From there dynein travels toward the MT minus ends. Note that a direct interaction between dynein and kinesin-1 is also possible and was shown in mammalians (42). (*B*) Kinesin-3 moves EEs in the anterograde direction toward the tip of the cell. On their way toward the MT plus ends the EEs meet retrograde moving dynein that can stochastically bind to the EEs. In a tug-of-war dynein takes over and turns the direction of motility. Kinesin-3 remains bound to the EEs but is unable to take the EEs back toward MT plus ends until dynein is released.

Indeed, during anterograde motility, only kinesin-3 is present on the organelle, whereas a change in transport direction depends on the binding and unbinding of dynein. Such a possibility of motility transitions due to changes in the size of the motor teams has been theoretically considered (13, 44). In principle, the dynein could be recruited from the cytoplasm. However, we never observed such recruitment from a soluble pool. Instead, dynein appears to be released from the comet-like reservoir at MT-plus ends (Fig. 6*A*) (36). We suggest here that this retrograde moving dynein meets EEs while they move to MT plus ends. Theoretical modeling further suggests that such a mechanism can account for the observed behavior of EEs (*SI Methods* and Fig. S5). The conceptual novelty of this mechanism is that the anterograde and retrograde run length of the organelles is determined by the stochastic binding and unbinding of dynein. In other words, the probability of dynein interacting with the EEs underlies the observed bidirectional behavior of the organelles.

In our system EEs carry one dynein and approximately three to five kinesin-3s. However, when dynein binds to EEs, it always changes the transport direction. Although these motor numbers are in agreement within reported numbers in other cell systems (7, 9, 10), their ratio is not. Bidirectional motility of lipid droplets in flies (9) and endosomal/lysosomal vesicles in primary neurons (7) is mediated by an almost even ratio of dyneins and kinesins. Furthermore, in the amoeba *Dictyostelium discoideum* EE transport is governed by a single kinesin-3 motor that counteracts numerous weaker dyneins (10). Possible explanations for the difference in *U. maydis* are that not all EE-bound kinesin-3 motors are active and therefore do not participate in a tug-of-war with dynein. Indeed, kinesin-3 numbers fluctuate while signals move along MTs, and under CCCP-induced ATP depletion only three of five kinesins tightly bind to MTs. Although it is possible that the CCCP treatment is not efficiently anchoring kinesin-3, these data might also indicate that some motors are not bound to the MTs and therefore do not compete with dynein during EE motility. However, the remaining three to four kinesins are predicted to be sufficient for long-range transport of cargo (*SI Methods*). Finally, motors from different cell types and organisms might operate differently and exert various forces. In *D. discoideum* one kinesin-3 produces 5–6 pN (10), whereas mammalian kinesin-3 (Kif1A) exerts a lower force (~2.5 pN) (45). Thus, we consider it possible that in *U. maydis* one strong dynein could overcome the few relatively weak kinesin-3 motors in a tug-of-war.

It is important to note that our analysis was done in living cells. Here, MTs bind numerous associated proteins, which could become obstacles for motor-based transport (46, 47) that can selectively inhibit kinesin attachment to MTs (48). It seems possible that such "roadblocks" occasionally interfere with retrograde EE trafficking, thereby causing the unbinding of dynein from the organelle. After dynein left the EEs, many organelles paused, which might reflect the time needed for kinesin-3 motors to rebind the MTs. Thus, long-range motility of EEs in *U. maydis* could be controlled by a series of events (Fig. 6*B*): (*i*) dynein stochastically binds to anterograde EEs and wins in a tug-of-war over kinesin-3; (*ii*) while dynein moves the EEs, most kinesin-3 motors are detached from the MTs and therefore unable to take over; and (*iii*) when the EE hits an obstacle, dynein falls off the EE and kinesin-3 rebinds to take the organelle back toward the plus ends. Such a mechanism is unique, as the stochastic binding and release of dynein limit the run length of kinesin-3 and thereby control EE motility. In this model, cargo-free dynein meets anterograde EEs on their way to the tip. Alternatively, dynein might be bound to some unknown retrograde cargo and the collision of EEs with this cargo–motor complex could trigger minus-end–directed motility. We currently cannot distinguish between these options, but for both mechanisms dynein needs to travel over long distances to meet the anterograde EEs. Indeed, we do find dynein signals moving over >30 µm in the retrograde direction. This run length significantly exceeds the distance dynein travels in vitro (49, 50). The molecular basis for this large run length of dynein is not known. Single-molecule studies on purified motors have shown that associated factors, such as dynactin, NudE, and Lis1, increase the processivity of dynein (49, 50). It remains to be seen whether these factors are required for dynein motility in *U. maydis* and whether a similar dynein-based mechanism controls long-range membrane transport in neurons.

Methods

Strains, Plasmids, and Growth Conditions. All *U. maydis* strains and plasmids are listed in the *SI Methods*, Table S2. Plasmids were constructed using standard techniques. *U. maydis* transformation techniques were described

elsewhere (26). Strains were grown at 28 °C in complete medium/1% glucose. Hyphal growth was induced by shifting to nitrate minimal medium supplemented with 1% glucose. Temperature-sensitive mutants were grown at 22 °C and shifted to 32 °C for 2 h before observation.

Microscopy and Image Analysis. Cells were observed using an IX81 microscope (Olympus) and a VS-LMS4 Laser-Merge-System (Visitron). Photoactivation and photobleaching experiments were performed using a 405-nm/60-mW diode laser. Colocalization was performed using a Dual-View Microimager (Photometrics) and appropriate filters. Images were captured using a Photometrics CoolSNAP HQ2 camera (Roper Scientific). The system was controlled by MetaMorph (Molecular Devices). All measurements and image processing were done using MetaMorph, and statistical analysis was done using Prism4 (GraphPad). ATP-depletion cells were induced by treatment with 100 μM CCCP (carbonyl cyanide 3-chlorophenylhydrazone; Sigma-Aldrich Ltd). Quantitative photobleaching experiments were done using the step-find algorithm (35) as previously described (36). Comparison of GFP_3-Dyn2 and Kin3-GFP with the nucleoporin Nup107-GFP as internal calibration standard followed published procedures (36). For more detailed information on all methods, see *SI Methods*.

ACKNOWLEDGMENTS. We thank G. Fink for establishing photoactivatable GFP-Rab5a, Dr. M. Feldbrügge for providing strain AB5Dyn2^{ts} that was used to generate strain AB5Dyn2^{ts}_paGRab5a, and Dr. Jacob Kerssemakers for help with the bleaching step analysis. This project was supported by Biotechnology and Biological Sciences Research Council Grant BB/F022956/1, Deutsche Forschungsgemeinschaft Grants STE 799/4-3 and SFB593, and the Max-Planck Institute for terrestrial Microbiology, Marburg, Germany.

1. Welte MA (2004) Bidirectional transport along microtubules. *Curr Biol* 14:R525–R537.
2. Gross SP (2004) Hither and yon: A review of bi-directional microtubule-based transport. *Phys Biol* 1:R1–R11.
3. Ally S, Larson AG, Barlan K, Rice SE, Gelfand VI (2009) Opposite-polarity motors activate one another to trigger cargo transport in live cells. *J Cell Biol* 187:1071–1082.
4. Vale RD (2003) The molecular motor toolbox for intracellular transport. *Cell* 112: 467–480.
5. Chevalier-Larsen E, Holzbaur EL (2006) Axonal transport and neurodegenerative disease. *Biochim Biophys Acta* 1762:1094–1108.
6. Gross SP, et al. (2002) Interactions and regulation of molecular motors in *Xenopus* melanophores. *J Cell Biol* 156:855–865.
7. Hendricks AG, et al. (2010) Motor coordination via a tug-of-war mechanism drives bidirectional vesicle transport. *Curr Biol* 20:697–702.
8. Welte MA, Gross SP, Postner M, Block SM, Wieschaus EF (1998) Developmental regulation of vesicle transport in Drosophila embryos: Forces and kinetics. *Cell* 92: 547–557.
9. Shubeita GT, et al. (2008) Consequences of motor copy number on the intracellular transport of kinesin-1-driven lipid droplets. *Cell* 135:1098–1107.
10. Soppina V, Rai AK, Ramaiya AJ, Barak P, Mallik R (2009) Tug-of-war between dissimilar teams of microtubule motors regulates transport and fission of endosomes. *Proc Natl Acad Sci USA* 106:19381–19386.
11. Kural C, et al. (2005) Kinesin and dynein move a peroxisome *in vivo*: A tug-of-war or coordinated movement? *Science* 308:1469–1472.
12. Laib JA, Marin JA, Bloodgood RA, Guilford WH (2009) The reciprocal coordination and mechanics of molecular motors in living cells. *Proc Natl Acad Sci USA* 106: 3190–3195.
13. Müller MJ, Klumpp S, Lipowsky R (2008) Tug-of-war as a cooperative mechanism for bidirectional cargo transport by molecular motors. *Proc Natl Acad Sci USA* 105: 4609–4614.
14. Gross SP, Welte MA, Block SM, Wieschaus EF (2002) Coordination of opposite-polarity microtubule motors. *J Cell Biol* 156:715–724.
15. Deacon SW, Nascimento A, Serpinskaya AS, Gelfand VI (2005) Regulation of bidirectional melanosome transport by organelle bound MAP kinase. *Curr Biol* 15: 459–463.
16. Guillaud L, Wong R, Hirokawa N (2008) Disruption of KIF17-Mint1 interaction by CaMKII-dependent phosphorylation: A molecular model of kinesin-cargo release. *Nat Cell Biol* 10:19–29.
17. Deacon SW, et al. (2003) Dynactin is required for bidirectional organelle transport. *J Cell Biol* 160:297–301.
18. Welte MA, et al. (2005) Regulation of lipid-droplet transport by the perilipin homolog LSD2. *Curr Biol* 15:1266–1275.
19. Larsen KS, Xu J, Cermelli S, Shu Z, Gross SP (2008) BicaudalD actively regulates microtubule motor activity in lipid droplet transport. *PLoS ONE* 3:e3763.
20. Steinberg G, Perez-Martin J (2008) *Ustilago maydis*, a new fungal model system for cell biology. *Trends Cell Biol* 18:61–67.
21. Hirokawa N, Noda Y, Tanaka Y, Niwa S (2009) Kinesin superfamily motor proteins and intracellular transport. *Nat Rev Mol Cell Biol* 10:682–696.
22. Schuchardt I, Assmann D, Thines E, Schuberth C, Steinberg G (2005) Myosin-V, Kinesin-1, and Kinesin-3 cooperate in hyphal growth of the fungus *Ustilago maydis*. *Mol Biol Cell* 16:5191–5201.
23. Wedlich-Söldner R, Bölker M, Kahmann R, Steinberg G (2000) A putative endosomal t-SNARE links exo- and endocytosis in the phytopathogenic fungus *Ustilago maydis*. *EMBO J* 19:1974–1986.
24. Hoepfner S, et al. (2005) Modulation of receptor recycling and degradation by the endosomal kinesin KIF16B. *Cell* 121:437–450.
25. Wedlich-Söldner R, Straube A, Friedrich MW, Steinberg G (2002) A balance of KIF1A-like kinesin and dynein organizes early endosomes in the fungus *Ustilago maydis*. *EMBO J* 21:2946–2957.
26. Lenz JH, Schuchardt I, Straube A, Steinberg G (2006) A dynein loading zone for retrograde endosome motility at microtubule plus-ends. *EMBO J* 25:2275–2286.
27. Fuchs U, Hause G, Schuchardt I, Steinberg G (2006) Endocytosis is essential for pathogenic development in the corn smut fungus *Ustilago maydis*. *Plant Cell* 18: 2066–2081.
28. Steinberg G (2007) On the move: Endosomes in fungal growth and pathogenicity. *Nat Rev Microbiol* 5:309–316.
29. Straube A, et al. (2001) A split motor domain in a cytoplasmic dynein. *EMBO J* 20: 5091–5100.
30. Zhang J, Li S, Fischer R, Xiang X (2003) Accumulation of cytoplasmic dynein and dynactin at microtubule plus ends in *Aspergillus nidulans* is kinesin dependent. *Mol Biol Cell* 14:1479–1488.
31. Ulbrich MH, Isacoff EY (2007) Subunit counting in membrane-bound proteins. *Nat Methods* 4:319–321.
32. Grishchuk EL, et al. (2008) Different assemblies of the DAM1 complex follow shortening microtubules by distinct mechanisms. *Proc Natl Acad Sci USA* 105: 6918–6923.
33. Hammond JW, et al. (2009) Mammalian Kinesin-3 motors are dimeric *in vivo* and move by processive motility upon release of autoinhibition. *PLoS Biol* 7:e72.
34. Hirose S, Yaginuma N, Inada Y (1974) Disruption of charge separation followed by that of the proton gradient in the mitochondrial membrane by CCCP. *J Biochem* 76: 213–216.
35. Kerssemakers JW, et al. (2006) Assembly dynamics of microtubules at molecular resolution. *Nature* 442:709–712.
36. Schuster M, et al. (2011) Controlled and stochastic retention concentrates dynein at microtubule ends to keep endosomes on track. *EMBO J*, 10.1038/emboj.2010.360.
37. Rogers SL, Tint IS, Fanapour PC, Gelfand VI (1997) Regulated bidirectional motility of melanophore pigment granules along microtubules *in vitro*. *Proc Natl Acad Sci USA* 94:3720–3725.
38. Ma S, Chisholm RL (2002) Cytoplasmic dynein-associated structures move bidirectionally *in vivo*. *J Cell Sci* 115:1453–1460.
39. Pedersen LB, Geimer S, Rosenbaum JL (2006) Dissecting the molecular mechanisms of intraflagellar transport in *chlamydomonas*. *Curr Biol* 16:450–459.
40. Scholey JM (2003) Intraflagellar transport. *Annu Rev Cell Dev Biol* 19:423–443.
41. Hirokawa N, Sato-Yoshitake R, Yoshida T, Kawashima T (1990) Brain dynein (MAP1C) localizes on both anterogradely and retrogradely transported membranous organelles *in vivo*. *J Cell Biol* 111:1027–1037.
42. Ligon LA, Tokito M, Finklestein JM, Grossman FE, Holzbaur EL (2004) A direct interaction between cytoplasmic dynein and kinesin I may coordinate motor activity. *J Biol Chem* 279:19201–19208.
43. Haghnia M, et al. (2007) Dynactin is required for coordinated bidirectional motility, but not for dynein membrane attachment. *Mol Biol Cell* 18:2081–2089.
44. Müller JI, Klumpp S, Lipowsky R (2008) Motility states of molecular motors engaged in stochastic tug-of-war. *J Stat Phys* 133:1059–1081.
45. Okada Y, Higuchi H, Hirokawa N (2003) Processivity of the single-headed kinesin KIF1A through biased binding to tubulin. *Nature* 424:574–577.
46. Telley IA, Bieling P, Surrey T (2009) Obstacles on the microtubule reduce the processivity of Kinesin-1 in a minimal in vitro system and in cell extract. *Biophys J* 96: 3341–3353.
47. Chai Y, Lipowsky R, Klumpp S (2009) Transport by molecular motors in the presence of static defects. *J Stat Phys* 135:241–260.
48. Vershinin M, Carter BC, Razafsky DS, King SJ, Gross SP (2007) Multiple-motor based transport and its regulation by Tau. *Proc Natl Acad Sci USA* 104:87–92.
49. King SJ, Schroer TA (2000) Dynactin increases the processivity of the cytoplasmic dynein motor. *Nat Cell Biol* 2:20–24.
50. McKenney RJ, Vershinin M, Kunwar A, Vallee RB, Gross SP (2010) LIS1 and NudE induce a persistent dynein force-producing state. *Cell* 141:304–314.